Mon. Not. R. Astron. Soc. **330,** 92–104 (2002)

Submillimetre sources in rich cluster fields: source counts, redshift estimates and cooling flow limits

Scott C. Chapman,[1]†★ Douglas Scott,[2] Colin Borys[2] and Gregory G. Fahlman[2,3]
[1]*Observatories of the Carnegie Institution of Washington, Pasadena, CA 91101,USA*
[2]*University of British Columbia, Department of Physics & Astronomy, Vancouver, BC V6T 1Z4, Canada*
[3]*Canada–France–Hawaii Telescope, Kamuela, HI 96743, USA*

Accepted 2001 October 15. Received 2001 October 3; in original form 2001 August 30

ABSTRACT

Recent submillimetre surveys have revealed a population of dusty, high-redshift sources of great cosmological significance for understanding dust-enshrouded star formation in distant galaxies, and for determining the origin of the far-infrared background. In this paper, we analyse nine rich cluster fields mapped at 850 and 450μm with the SCUBA array on the James Clerk Maxwell Telescope. Lensing models of the clusters are developed in order to derive accurate source counts for our sample. VLA maps of the same clusters are used to help constrain the redshift distribution of our SCUBA detections. Implications for high-redshift galaxies and for the far-infrared background are discussed. We also provide limits on distributed dust produced by cooling flows in these clusters.

Key words: gravitational lensing – cooling flows – galaxies: evolution – galaxies: formation – infrared: galaxies – submillimetre.

1 INTRODUCTION

The submillimetre waveband has recently become an invaluable tool for investigating the properties of high-redshift galaxies. An early result using the Submillimetre Common User Bolometer Array (SCUBA: Holland et al. 1999) by Smail, Ivison & Blain (1997) showed that a much larger population of dusty, high-redshift galaxies existed than previously thought. The existence of these dusty, submillimetre galaxies at relatively high redshifts has now been confirmed in several surveys (Hughes et al. 1998; Barger et al. 1998, 1999a; Eales et al. 1999; Lilly et al. 1999a; Blain et al. 1999a). Such submillimetre sources could be of great cosmological significance – they may comprise a substantial fraction of the far-infrared background (FIRB: Puget et al. 1996; Hauser et al. 1998; Lagache et al. 1999). Additionally, they could be an important source of cosmic microwave background (CMB) anisotropy at arcsecond scales (Scott & White 1999). They are certainly the dominant source of sky fluctuations on arcsecond angular scales at wavelengths ~ 1 mm, at least out of the Galactic plane (Hughes et al. 1998; Borys, Chapman & Scott 1999). Our understanding of the star formation history of galaxies depends critically on the properties of these submillimetre sources: this population is responsible for a substantial fraction of the total star formation output in the early Universe, and holds important information about how galaxies formed and evolved (e.g. Blain & Longair 1993; Guiderdoni et al. 1997; Blain, Ivison & Smail 1998). They appear to be the high-redshift counterparts of well-studied nearby ultraluminous infrared galaxies (Sanders & Mirabel 1996), and can be plausibly interpreted as the formation sites of galactic spheroids through mergers of gaseous disc systems (e.g. Sanders 1999; Lilly et al. 1999a).

Much work has gone into identifying just what types of galaxies make up this submillimetre-bright population, and what mechanisms may be responsible for their rest-frame far-infrared emission (Smail et al. 1998; Hughes et al. 1998; Ivison et al. 1998b, 2000; Frayer et al. 1998, 1999, 2000; Lilly et al. 1999b; Chapman et al. 1999, 2000; Bertoldi et al. 2000; Gear et al. 2000). However, the numbers of submillimetre source detections are still relatively small. In an effort to increase the statistics and broaden the source count baseline, we have undertaken a submillimetre survey including both blank sky (Borys et al., in preparation) and cluster fields. Our cluster sample is complementary to that of Smail et al. (1997, 1998) who pioneered this approach using SCUBA on the James Clerk Maxwell Telescope (JCMT). These cluster fields benefit from lensing by the foreground cluster mass at $z < 1$, enhancing sensitivity to the dusty galaxies at higher redshifts.

Our cluster sample consists of nine clusters at redshifts 0.2–0.8, originally selected to search for both distributed cool dust (cooling flows: see Edge et al. 1999) and the Sunyaev–Zel'dovich (SZ) effect (Birkinshaw 1999; Andreani et al. 1999). Although we found no convincing evidence for distributed emission, our SCUBA maps have revealed significant source detections, as expected from the counts from other surveys (e.g. Blain et al. 1999; Barger, Cowie & Sanders 1999b). This further demonstrates that submillimetre

★E-mail: schapman@mop.caltech.edu
†Present address: California Institute of Technology, 1200 E. California Blvd, Pasadena, CA 91125, USA.

surveys provide an efficient means of identifying a population of dusty active galactic nuclei (AGN) and/or star-forming galaxies, possibly at very high redshifts. In addition, a few weak sources appear coincident with radio-bright central galaxies in the clusters, possibly associated with the strong cooling flows suggested by the X-ray profiles. In this paper, we describe possible sources found in the cluster fields, and present the resulting source counts. Existing VLA maps are used to place limits on the redshift distribution of the sample. We conclude by discussing the implications for high-redshift galaxies and the FIRB.

2 OBSERVATIONS

2.1 JCMT data

Nine clusters were observed with the SCUBA instrument on the JCMT, resulting in 17 significant source detections greater than 3σ. During four observing runs throughout 1998 and 1999, we operated the 91-element short-wave array at 450μm, and the 37-element long-wave array at 850μm simultaneously, in JIGGLE mode, and additionally the single photometry pixel at 1350μm for some sources, giving half-power beamwidths of 7.5, 14.7 and 21.0 arcsec respectively. Additionally, 850/450-μm PHOTOMETRY mode follow-up on three of the sources was performed, confirming their existence and flux densities. The central pixel of SCUBA was fixed on the source, as defined by the centroid of the *ROSAT* imaging (Crawford et al. 1999). For mapping, the standard 64-point jiggle pattern was employed to sample fully the 450- and 850-μm arrays. The effective integration times (time spent on- and off-source derived from the number of 64-point integrations obtained, which excludes overheads) are presented in Table 1 for each cluster. For 1350-μm photometry we used the nine-point jiggle pattern to reduce the impact of pointing errors by averaging the source signal over a slightly larger area than the beam, resulting in greater photometric accuracy. Whilst jiggling, the secondary was chopped at 7.8125 Hz with chop throws between 40 and 120 arcsec in azimuth, with smaller throws used under worse atmospheric conditions or when the projected core radius for a cluster was smaller.

Pointing was checked hourly on blazars, and sky-dips were performed to measure the atmospheric opacity directly. The rms pointing errors were below 2 arcsec, while the average atmospheric zenith opacities at 450, 850 and 1350μm were fairly stable and generally quite good with τ_{850} ranging from 0.15 to 0.36. Some short-time-scale variations, presumably caused by the atmosphere, caused some parts of the data set to be noisier, and these noisiest sections were excluded.

The data were reduced using the Starlink package SURF (Scuba User Reduction Facility: Jenness, Lightfoot & Holland 1998). Spikes were first carefully rejected from the data, followed by correction for atmospheric opacity and sky subtraction using the median of all the array pixels, except for obviously bad pixels (the 1350-μm pixel currently has no provision for subtracting sky variations using the other wavelength pixels). We then weighted each pixel by its timestream inverse variance, relative to the central pixel. Multiple scans on the same cluster field, and sky rotation, ensure that (in most cases) each point of the map is covered by many bolometers. Even with the inverse variance weighting, excessively bad pixels still appeared to degrade the map, and were therefore clipped from the data prior to rebinning into the final maps. The data were then calibrated against standard planetary or compact H II region sources, observed during the same nights as the clusters. Uncertainties at 850 and 1350μm are estimated to be around 10 per cent, while at 450μm they could be as high as 25 per cent. Note that calibration uncertainties do not affect the signal-to-noise ration (S/N) level for our detections, only the overall flux densities reported.

2.2 Archive VLA data

VLA maps at 4.9 GHz in the C configuration were obtained for five clusters in our sample, courtesy of A. Edge. The effective resolution in the images is 5 arcsec. More details of the reduction and analysis of similar maps are given in Edge et al. (1999). Typical 1σ sensitivities lie around 60μJy. In addition, an archive 1.4-GHz map for Abell 2219 was obtained courtesy of F. Owen, reaching a 1σ limit of $\sim$39μJy per 2-arcsec beam.

For the remaining clusters, VLA data presented by Stocke et al. (1999) at 1.4 GHz in the B configuration were used to set limits and identify counterpart positions. Typical 1.4-GHz sensitivities in these maps are 65μJy rms.

3 SOURCE CATALOGUE

The 850-μm SCUBA maps for the clusters showing significant

Table 1. Submillimetre observations for the clusters in our sample.

Cluster	RA[a] (J2000)	Dec.[a] (J2000)	z	Exposure time (ks)	S_{850}[b](1σ) (mJy)	S_{450}[b](1σ) (mJy)	$N(S_{850} > S_{\rm lim})$ 3σ	4σ
Cl 0016 + 16	00 18 33.2	+ 16 26 18	0.541	20.5	3.1	36	2	0
MS 0451 − 03	04 54 13.4	− 03 01 47	0.550	14.1	4.2	181	2	2
Abell 520	04 54 19.0	+ 02 56 49	0.203	7.7	5.0	66	2	1
Zwicky 3146	10 23 39.6	+ 04 11 10	0.291	12.8	2.6	25	4	1
MS 1054−03	10 57 00.2	− 03 37 27	0.833	7.7	4.3	103	1	0
MS 1455 + 22	14 57 15.1	+ 22 20 35	0.259	15.4	2.1	22	1	1
Abell 2163	16 15 34.1	− 06 07 26	0.201	7.7	5.8	44	0	0
Abell 2219	16 40 20.5	+ 46 42 59	0.228	15.4	1.7	8	4	1
Abell 2261	17 22 24.1	+ 32 07 45	0.224	7.7	3.8	105	1	1
Total							17	7

[a]*X*-ray centre – *ROSAT* archive.
[b]Measured rms over the central 60 arcsec of the field after subtracting a scaled SCUBA beam profile from any identified sources in the region.

source detections are presented in Figs 1 and 2. Any real objects in our maps are expected to be unresolved and will typically appear as a positive point spread function with FHWM $\sim$15 arcsec at 850μm. For most of our maps, we do not expect to see negative signatures for our sources, as the individual scans coadded in the map have different chop throws and directions, diluting the effect of off-beams. We also chopped out of the field in most cases. The edges of the maps incur a rapid rise in noise level owing to incomplete sampling of the sky for the outer bolometers of the SCUBA array. Eales et al. (1999) simulated the incomplete sampling at the field edge and found that any spurious sources in Monte Carlo simulations tended to appear in this region. We have therefore clipped the 14-arcsec edge regions in our maps where the noise level increases by a factor of $\gtrsim 2$ relative to that at the field centre.

As the S/N is low for individual pixels, we use a template fitting method for source detection to achieve a maximum gain in S/N, similar to that used by Eales et al. (1999). The cluster maps are convolved with the beam map obtained by imaging Mars, and all peaks greater than 3σ are extracted as potential sources. We checked the convolved maps carefully against the raw data to ensure that no residual bad pixels were identified as sources. We also note that there are no strong negative sources in our maps.

Sensitivity limits for deep SCUBA integrations have now been fairly well characterized (Smail et al. 1997; Hughes et al. 1998; Eales et al. 1999; Barger et al. 1999b). At these low S/N levels, however, we must be careful to consider possible systematic noise effects. There are currently five identified components that contribute to the overall SCUBA noise level: (i) photon noise from the sky; (ii) telescope and instrumental noise; (iii) blanked-off

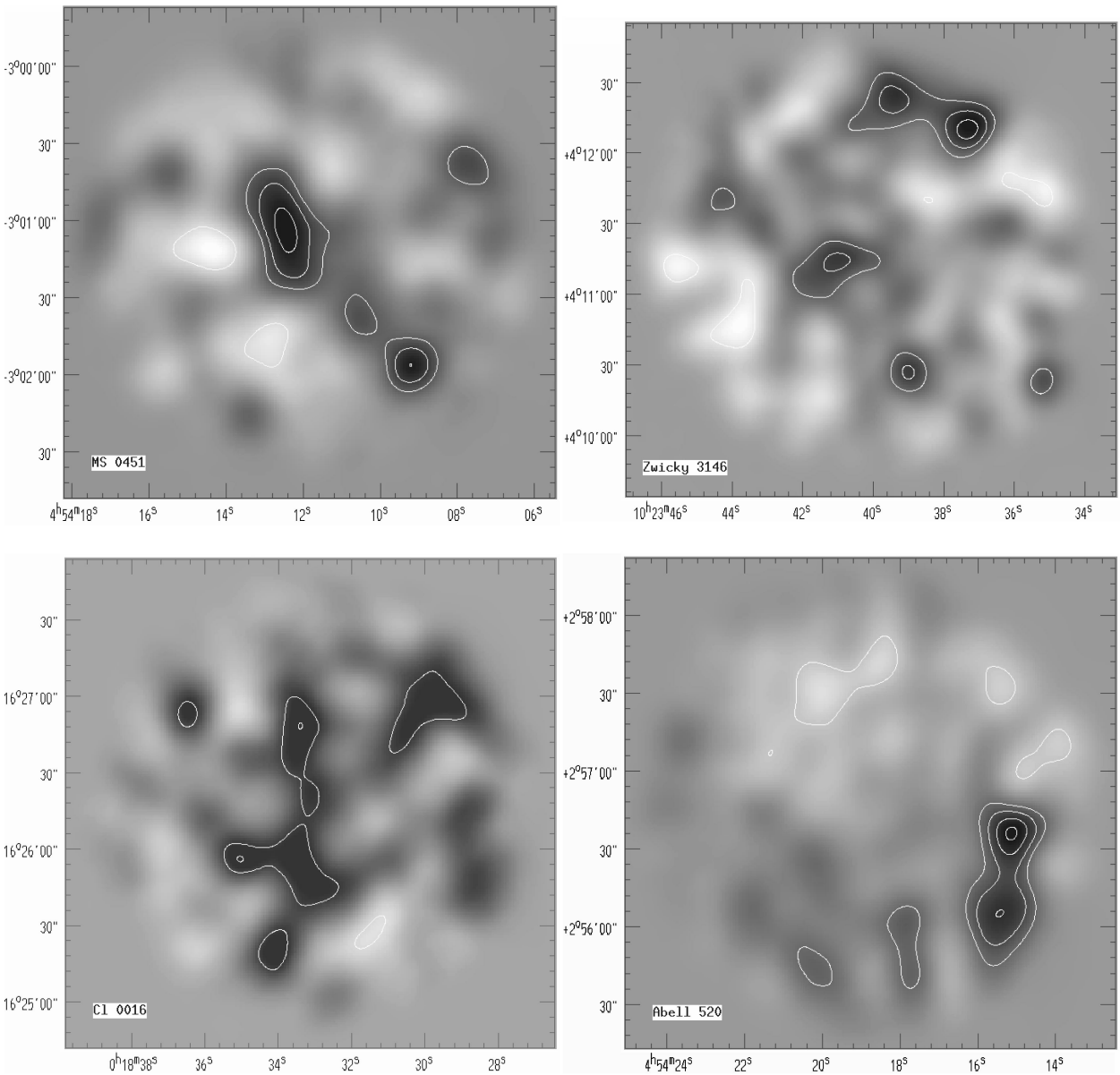

Figure 1. Cluster field images at 850μm, convolved with the SCUBA 14.7-arcsec beam. Dark shading is positive flux density, while lighter shading is negative.All contour levels indicate the number of sigma above the background noise estimated from the central regions of the beam-convolved images, starting at 2σ, with intervals of 1σ. These noise levels correspond approximately to the tabulated values (Tables 1 and 2), which were derived from the raw data. Top row: MS 0451−3 (left); Zwicky 3146 (right). Bottom row: C10016 + 16 (left); Abell 520 (right).

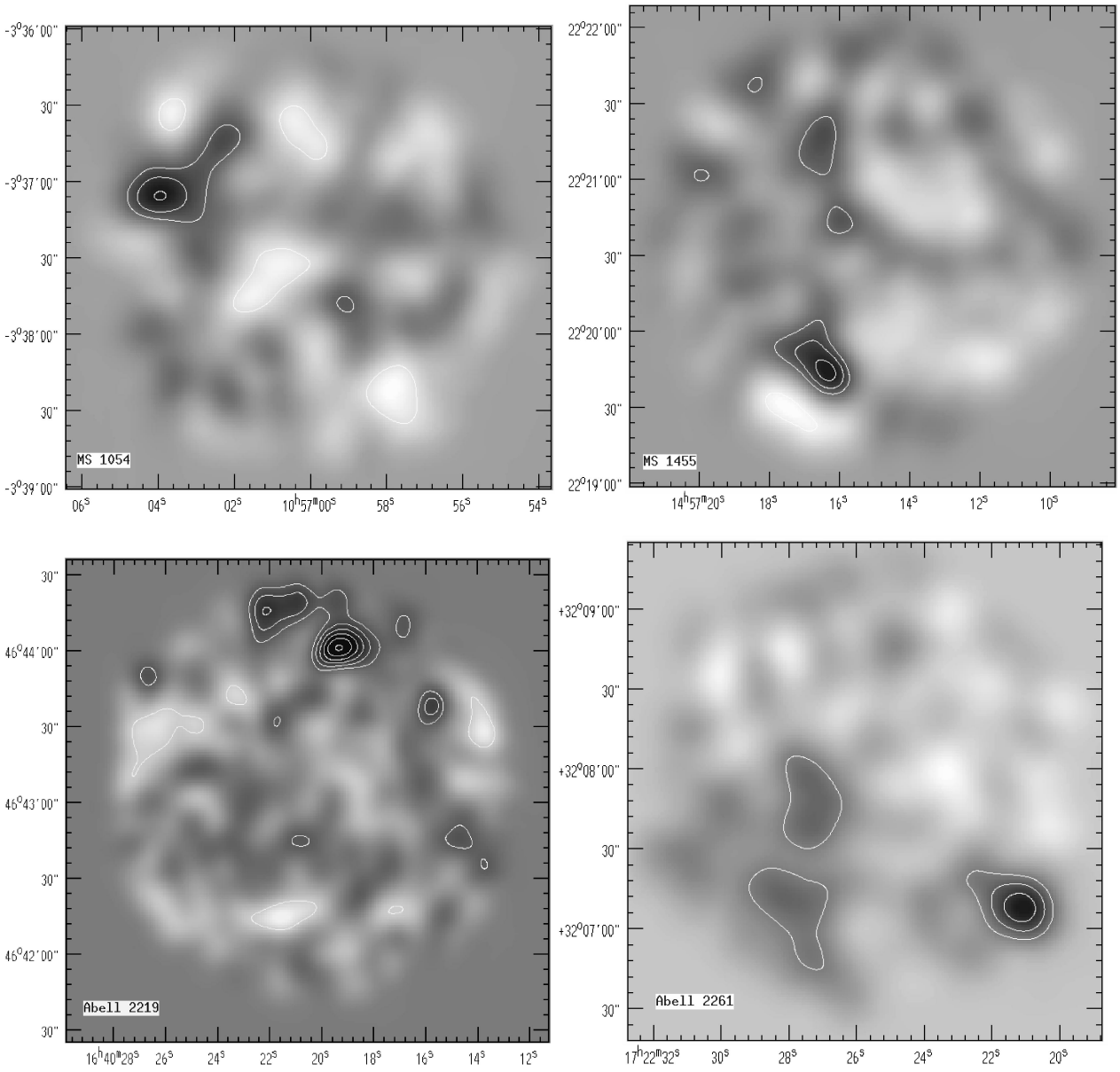

Figure 2. SCUBA maps at 850μm (continued). Contours are the same as in Fig. 1. Top row: MS 1054−03 (left); MS 1455 + 22 (right). Bottom row: Abell 2219 (left); Abell 2261 (right).

detector Johnson, phonon and amplifier noise; (iv) excess photon noise from the optics; (v) excess radiative load in the dewar. The noise terms add in quadrature, and the estimates for the relative contributions at the average sky emissivity for our survey ($\langle\tau_{850}\rangle \simeq 0.2$) are respectively 29, 25, 17, 13 and 16 per cent (W. Holland, private communication). Thus sky noise is the largest source, but does not dominate the others. Nevertheless, we expect the noise to integrate down with time. This will not be true of one additional source of noise: 'confusion noise' arising from fluctuations due to undetected sources. However, the level is essentially negligible for these observations – Blain et al. (1998) quote a value of $\sigma_{\rm conf} = 0.44$ mJy, derived from their source counts, while we find that any reasonable extrapolation of the counts (together with the constraint of not over-producing the FIRB) leads to a variance of no more than 0.5 mJy. We can therefore safely ignore confusion noise. However, it is worth pointing out that lensing by the clusters effectively allows us to probe below the confusion limit of, say, $3\sigma_{\rm conf}$.

With transient noise and bad pixels from scan to scan, our confidence in many of the detections is reinforced by dividing the data into two parts and seeing evidence of the sources (at the $>2\sigma$ level) appear in both. Multi-wavelength detections also substantially strengthen our confidence in a source. Although the 450-μm channel is typically not sensitive enough to detect these objects, especially those lying at higher redshifts, many more of them may be observable at 1350μm with deeper photometry than we have currently obtained. Three sources have been subsequently verified through PHOTOMETRY follow-up observations (MS 0451-A, Abell 2261-A and MS 1455-A). These are discussed in Section 4.2.

Empirically, the localized noise levels are seen to integrate down in our maps roughly as $t^{-1/2}$ (see also Ivison et al. 1998a). We note that in a typical 850-μm SCUBA field of 5.2 arcmin^2 with ~ 100 independent beams we expect only ~ 0.1 spurious 3σ peaks from Gaussian noise, and $\ll 1$ spurious 4σ peak from our whole survey.

The completeness of a set of detections has typically been established using synthetic source recovery techniques in Monte Carlo simulations (Smail et al. 1997; Hughes et al. 1998). Our 3σ and source catalogues correspond approximately to the 80 per cent completeness level found by Smail et al. (1997). We estimate that our 4σ catalogue is more than 90 per cent complete.

Our submillimetre observations of the clusters are presented in Tables 1 and 2. Table 1 lists the clusters, coordinates and redshifts, along with total exposure time (based on the number of integrations). The last four columns present the average 850- and 450-μm sensitivities achieved after subtracting sources $> 3\sigma$ from the field, and the number of sources detected at greater than the 3σ and 4σ levels. Table 2 lists the properties of the detected sources, with coordinates and observed flux densities in each of the three submillimetre wavelength bands. These submillimetre detections and upper limits (upper limits are given as 95 per cent Bayesian confidence regions, assuming Gaussian errors and neglecting the negative flux region) at 1350, 850 and 450μm provide rough photometric estimates of the source redshifts (see e.g. Hughes et al. 1998). However, the addition of radio data significantly increases confidence in these photometric redshifts. The final two columns list the VLA radio flux limits, and estimates of the redshift from the submillimetre and radio data, as described below.

4 PROPERTIES OF INDIVIDUAL SOURCES

4.1 VLA radio counterparts

Radio counterparts to submillimetre sources are expected because of the synchrotron emission resulting from either an AGN or shocked gas in supernova remnants from a starburst (e.g. Richards, Fomalont & Kellermann 1999). Given the small number density of radio-emitting objects, the chances of finding a 1.4-GHz VLA object of >200μJy in our error circle by chance are much less than 1 per cent (Richards et al. 1998). By contrast, identifying optical counterparts to the SCUBA-selected galaxies is a non-trivial matter for two main reasons: (1) the beamsize at 850μm (the optimal wavelength for these studies) is ~ 15 arcsec, with pointing errors

Table 2. Details of individual sources.

Source	RA[a] (J2000)	Dec.[a] (J2000)	$S_{1350\mu m}$[b] (mJy)	$S_{850\mu m}$[b] (mJy)	$S_{450\mu m}$[b] (mJy)	$S_{1.4\,GHz}$[c] (μJy)	z_{est}[d]
Cl 0016							
A SMMJ00186 + 1626	00 18 35.2	+ 16 25 58		9.9 ± 3.3	7 ± 34	< 200	> 1.8
B SMMJ00186 + 1625	00 18 34.1	+ 16 25 20		9.8 ± 3.2	− 4 ± 36	< 200	> 1.8
MS 0451							
A SMMJ04541 − 0302	04 54 09.0	− 03 01 57		16.8 ± 4.2	24 ± 181	< 200	> 2.2
B SMMJ04542 − 0301[g]	04 54 12.5	− 03 01 04		19.1 ± 4.2	− 61 ± 177	< 200	> 2.3
Abell 520:							
A SMMJ04543 + 0257	04 54 15.2	+ 02 56 35		33.0 ± 5.0	− 39 ± 67	< 420	> 2.2
B SMMJ04543 + 0256	04 54 15.5	+ 02 56 05		16.2 ± 5.1	13 ± 70	< 410	> 1.6
Zwicky 3146							
A SMMJ 10237 + 0411	10 23 41.1	+ 04 11 17	1.7 ± 3.9	9.3 ± 2.5	15 ± 23	482/2722[e]	1.1/0.3[e](< 10)
B SMMJ 10237 + 0410	10 23 39.3	+ 04 10 29		9.2 ± 2.5	− 2 ± 25	543	1.1
C[h] SMMJ 10237 + 0412	10 23 39.4	+ 04 12 24		9.4 ± 3.1	6 ± 27	< 450	> 1.2
D[h] SMMJ 10236 + 0412	10 23 37.5	+ 04 12 08		11.2 ± 3.1	23 ± 27	467	1.3
MS 1054							
A SMMJ 10571 − 0337	10 57 04.0	− 03 37 07	15.2 ± 5.4	14.8 ± 4.3	12 ± 103	< 200/1600	2.1/0.8(10)
MS 1455:							
A SMMJ 14573 + 2220[g]	14 57 16.4	+ 22 19 39		10.1 ± 2.2	5 ± 22	< 294	> 1.5
Abell 2219							
A SMMJ 16403 + 46440	16 40 19.4	+ 46 44 01	4.3 ± 2.0	10.6 ± 1.7	34 ± 11	< 220	> 1.8(6)
B SMMJ 16403 + 46437	16 40 15.8	+ 46 43 39		5.8 ± 1.7	− 2 ± 8	593	0.8
C SMMJ 16404 + 4643	16 40 21.0	+ 46 42 45		< 5.7	26 ± 8	280/9100	0.9/0.2
D SMMJ 16404 + 4644	16 40 22.2	+ 46 44 13		6.3 ± 2.0	n/a[f]	1270	0.4
Abell 2261							
A SMMJ 17223 + 3207[g]	17 22 20.8	+ 32 07 04		17.6 ± 3.9	− 56 ± 105	< 452	> 1.6

[a]Positional errors for SCUBA sources with identifications at radio and optical wavelengths (e.g. Ivison et al. 1998b; Frayer et al. 1999) are ~ 6 arcsec for 4σ detections and ~ 8 arcsec for 3σ detections.
[b]Estimated flux densities with 1σ errors. All non-detection upper limits are given as 95 per cent Bayesian confidence regions, assuming Gaussian errors and neglecting the negative flux region.
[c] Bayesian 95 per cent limits at 1.4 GHz for sources in A520, Zw 3146, MS 1455, A2219 and A2261 have been extrapolated from the value at 4.9 GHz, using a spectral index $\alpha = 0.8$ appropriate for star formation driven synchrotron emission. For the data from Stocke et al. (1999), only 3σ upper limits are given.
[d] Redshift estimate using CY radio/far-infrared correlation.
[e] In cases where there is ambiguity between the central cluster galaxy and a background galaxy, the radio flux of the cluster galaxy is also listed, and the cluster redshift is given after the radio-estimated redshift. For those sources with 1350-μm detections or limits, the redshift estimated from the 1350/850 ratio is given in brackets (see Section 4.2 for discussion).
[f]This source falls at the very edge of the short-wavelength array.
[g]These sources were verified with 850/450-μm photometry. See text for details.
[h] These sources, lying near the edge of the Zw 3146 field, were *not* verified after follow-up pointed 850/450-μm photometry measurements (see text for details).

for the telescope of order 2 arcsec; (2) the large, negative *K*-corrections (i.e. increase in flux density as the objects are redshifted) of dusty star-forming galaxies at these wavelengths imply that submillimetre observations can detect such objects at $z > 1$ in an almost distance-independent manner. Thus several candidate optical galaxies are often present within the uncertainty of the submillimetre detection, along with the possibility that the actual counterpart is at much higher redshift and undetectable with current optical imaging. In this paper we restrict our attention to radio counterparts, and defer detailed optical analysis of the submillimetre source positions to a separate paper.

Carilli & Yun (1999, 2000, hereafter CY) recently demonstrated that crude redshift estimates for distant dusty galaxies could be obtained in the absence of an optical counterpart using the spectral index between the submillimetre (850μm) and radio (1.4 GHz) wavebands ($\alpha_{1.4}^{850}$), with a mean galaxy model parametrized as $z = 0.050 - 0.308\alpha + 12.4\alpha^2 - 23.0\alpha^3 + 14.9\alpha^4$. The model spectral energy distributions (SEDs) used by CY are based largely on lower redshift observations; however, they are able successfully to describe the few high-redshift galaxies that have multi-wavelength radio and submillimetre observations available. Dunne, Clements & Eales (2000) have expanded the estimator to a larger sample of local *IRAS*-selected galaxies observed directly at 850μm. Follow up studies by Blain (1999) have shown that if lower dust temperatures are adopted for the submillimetre population than are seen in the local sources used in CY's models, then the allowed redshifts are slightly lower for a given value of $\alpha_{1.4}^{850}$. The isolated cases that do not fall within the CY model predictions are known to have strong radio-loud AGN components. The important point is that the derived redshift provides a lower limit, irrespective of the nature of the emission mechanism, AGN or starburst, since an AGN contribution to the radio emission flattens the radio spectrum, decreasing the redshift limit of the source. The modest scatter between the models in CY suggests that the $\alpha_{1.4}^{850}$ technique currently provides the most useful limit on the redshifts of submillimetre galaxies, in the absence of an optical counterpart.

Smail et al. (2000) recently applied the CY analysis to deep radio observations of the complete sample of SCUBA-selected galaxies from their cluster lens survey (Smail et al. 1998; Ivison et al. 2000), revealing a higher redshift distribution than previously expected from optical follow-up work. Using existing VLA data for our SCUBA cluster sample, we can thus constrain the redshift distribution of our population and set the stage for optical/near-infrared follow-up identifications.

We searched for radio counterparts around the nominal positions of the submillimetre sources based on the SCUBA astrometry. Positional errors have been well characterized for the SCUBA sources from the literature that were clearly identified in at least radio wavelengths, and in several cases optical and millimetre-interferometric observations (e.g. Ivison et al. 1998b; Frayer et al. 1999). Plausible counterparts were found within ∼ 6-arcsec-diameter circles for 4σ detections and ∼8-arcsec circles for 3σ detections, and we use similar error circles for our analysis. Eales et al. (2000) ran Monte Carlo simulations of their SCUBA mapping data and discovered that positional shifting at a typical level of ∼ 2 arcsec occurred as a result of noise plus confusion, with even larger offsets for the fainter sources.

Radio limits at 1.4 GHz for sources in A520, Zw 3146, MS 1455 and A2261, have been extrapolated from the value at 4.9 GHz, using a spectral index $\alpha = 0.8$ (i.e. $S \propto \nu^{-0.8}$) appropriate for star formation driven synchrotron emission. This provides a reasonable estimate of the source redshift using the CY relation (since a brighter radio counterpart leads to a lower redshift estimate, while an AGN component will flatten the spectrum giving rise to a higher redshift). The 1.4-GHz VLA data from Stocke et al. (1999) were used to derive limits for Cl 0016, MS 0451 and MS 1054, and an archive 1.4-GHz map of A2219 (courtesy of F. Owen) was used to measure fluxes directly. In five cases, there were radio sources $> 3\sigma$ lying within the error circle of the submillimetre beam. One of these may be a central cluster galaxy and is also discussed in the following section. The 15×15 arcsec^2 regions surrounding the submillimetre sources are shown in Fig. 3, with the apparent radio flux densities or limits listed in Table 2.

We use the CY relation (which is consistent with dust temperature $T_d = 50$ K) to generate these lower limits to the source redshifts. We note that the actual dust temperatures in the submillimetre sources may be lower, bringing down the redshifts, or of course higher, thereby raising the inferred redshifts. In general the constrained quantity is $T_d/(1+z)$.

4.2 Source verifications, characteristics and evidence for cluster members

We now discuss each cluster field in detail.

4.2.1 Cl 0016 + 16

The data for this cluster show a general positive excess at the $\sim 2\sigma$ level, with two peaks barely reaching the 3σ level in the convolved map (sources A and B). There are no 1.4-GHz VLA counterparts down to the 200-μJy level, although the bright 2.7-mJy radio source from Stocke et al. (1999) lies on a clear submillimetre peak which reaches 2.6σ significance in the convolved map. The generally positive excess could be caused by a Sunyaev–Zel'dovich increment (core radius ∼ 2 arcmin: Carlstrom et al. 1999), which is too noisy in this map to detect with any confidence. However, it may have some effect on the detectability of other sources in this field.

4.2.2 MS 0451 − 03

An unresolved source (B: SMMJ 04542 − 0301) is found to the west in this cluster, and there is north–south extended positive submillimetre emission over the X-ray centroid region, reaching 4σ in the convolved map (A: SMMJ 04541 − 0302). An additional 850-μm photometry observation centred on the elongated source reveals a detection of 10.1 ± 3.0 mJy, which is consistent with the peak flux densities found along the source as well as the positional accuracy of the SCUBA map. This central source is offset by 20 arcsec to the east from the brightest cluster galaxy (BCG), and 20 arcsec to the west from a 1.8-mJy VLA source (Stocke et al. 1999). This detection could possibly represent cool dust associated with a cooling flow or could be associated with the Sunyaev–Zel'dovich effect – in either case the emission would have to be very strong and isolated to a small region of the cluster. For this particular cluster, the in-field chop reveals signs of the negative beams. However, another map of this cluster, observed with a large chop for Sunyaev–Zel'dovich increment measurement (Halpern et al., in preparation), suggests that additional source structure in the central region would significantly distort a clear off-beam signature. The extended nature of this central source (also verified in our independent map) is most likely to be a blend of two or more sources. For the purposes of Table 2 we treat this as a single source. Positions and flux density estimates for such blends should be

treated with some caution until higher resolution images are available.

4.2.3 *Abell 520*

A large gradient appears to be present across the field, as evidenced by the increased positive excursions in the lower halves of both the 450- and 850-μm images and negative excursions in the upper half. This could be either real or due to some residual atmospheric signal – we could not find a convincing way to tell from our data, although we suspect the latter explanation. An apparent 4σ source (B: SMMJ 04543 + 0256) lying to the south of the primary source (A: SMMJ 04543 + 0257) is $\sim 3\sigma$ above the noise even once a linear gradient is fitted to the plane and subtracted. The flux density presented in Table 2 for this source reflects the subtraction of this linear gradient component. Both of these sources appear clearly in either half of the data set, although the exposure time is less in this field than in our other fields. There is no detection of either the BCG or the bright radio source lying to the east in the archive VLA map.

4.2.4 *Zwicky 3146*

The central source in Zw 3146 (A: SMMJ 10237 + 0411) appears to be extended east–west, and may be another blend. The VLA map (Fig. 4) reveals that the western extent of the SCUBA source is associated with the BCG, with fairly bright radio emission ($S_{1.4\,\mathrm{GHz}} = 0.92$ mJy). However, the eastern part of the SCUBA source shows no radio emission ($< 210\mu$Jy), and the CY analysis suggests a high-redshift background source. Sources B and C in this cluster field also have weak 4.9-GHz detections in the archive VLA map. We were unable to detect sources C and D with 850/450 − μm pointed photometry, and we regard them as potentially spurious. These sources do not enter our 4σ source count, and thus do not affect the interpretation of our sample properties.

4.2.5 *MS 1054−03*

The source in the MS 1054 field (A: SMMJ 10571 − 0337) has a 1350/850-μm flux density ratio near unity. As thermal dust emission alone would produce a steep $\propto \nu^{3.5}$ spectrum, this may indicate that the object has a flat-spectrum AGN radio contribution at 1350 μm, and perhaps at 850μm as well. A more extreme alternative is that the source actually lies at $z \sim 10$ where the 850- and 1350-μm points would lie near the dust peak. A bright VLA counterpart, offset by 15 arcsec from the submillimetre peak, has been identified by Condon et al. (1998) as a cluster AGN radio source, and the CY relationship is consistent within errors with the source lying in the cluster at $z \sim 0.8$. However, such a large radio/submillimetre offset is unlikely (see, for example, Richards et al. 1999), and SMMJ 10571−0337 could easily be a background galaxy lensed by the cluster. Within errors, the 1350/850-μm ratio is not inconsistent with a higher redshift source. This source has been verified in another SCUBA map of this cluster, although at a slightly lower flux level (P. van der Werf, private communication).

4.2.6 *MS 1455+22*

There is some evidence for 850-μm SCUBA flux associated with

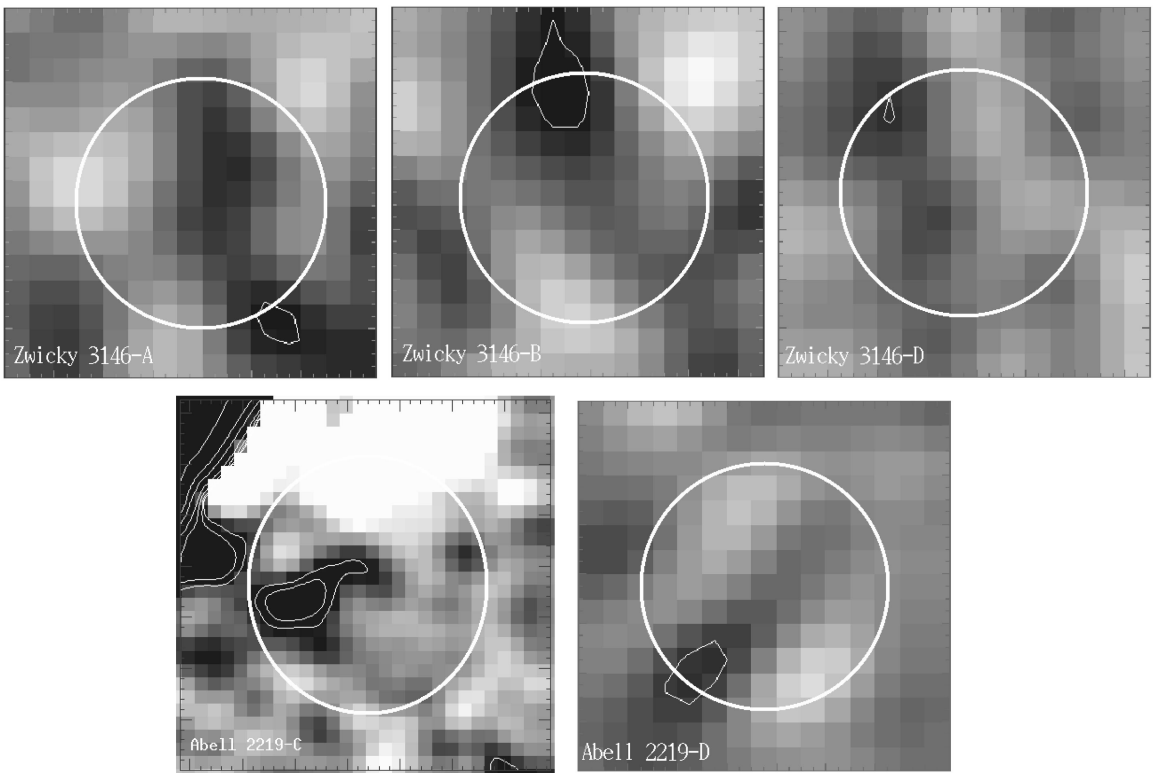

Figure 3. VLA counterparts to our submillimetre-detected galaxies. We show VLA sources for cases where a $> 3\sigma$ VLA detection is seen relatively near the SCUBA position. The radio contours are at 3, 5, 10, 20, 50, 100 and 200σ in all cases. The circles are drawn at the positions of sources (see Table 2) from our $> 3\sigma$ SCUBA source catalogue, with 10 arcsec diameter as an estimate of the positional uncertainty. The radio maps are at 4.9 GHz except for Abell 2219-C which is at 1.4 GHz. The other 12 SCUBA sources have only VLA upper limits, as listed in Table 2.

the BCG in the raw MS 1455 maps. However, a somewhat noisy central pixel during the observations of this cluster skews the peak profiles sufficiently that our source-finding routine does not identify this as a detection (the source appears at only 2.6σ in the final convolved map). We do not include this as a source in our catalogue until it can be verified. However, the proximity of the submillimetre peak to two bright radio sources (Fig. 4), and a possible CO(1–0) detection for the BCG (Edge et al., in preparation), lends credence to this putative source. The bright submillimetre source to the south (A: SMMJ 14573 + 2220) has no VLA counterpart in the archive maps. An additional 850-μm photometry observation centred on source A reveals a detection of 6.8 ± 1.8 mJy, which is consistent with the relative errors between the mapping and photometry measurements. The extended nature of this source could also yield a lower flux estimate from the single-beam photometry estimate, if the source were not centred in the beam.

4.2.7 *Abell 2163*

No sources were found in this cluster field down to a 3σ sensitivity of 17 mJy (corresponding roughly to 6 mJy after correction for lensing). This cluster had the poorest sensitivity, and we include it here for completeness only.

4.2.8 *Abell 2219*

This map has by far the lowest 450-μm rms, and as a result there

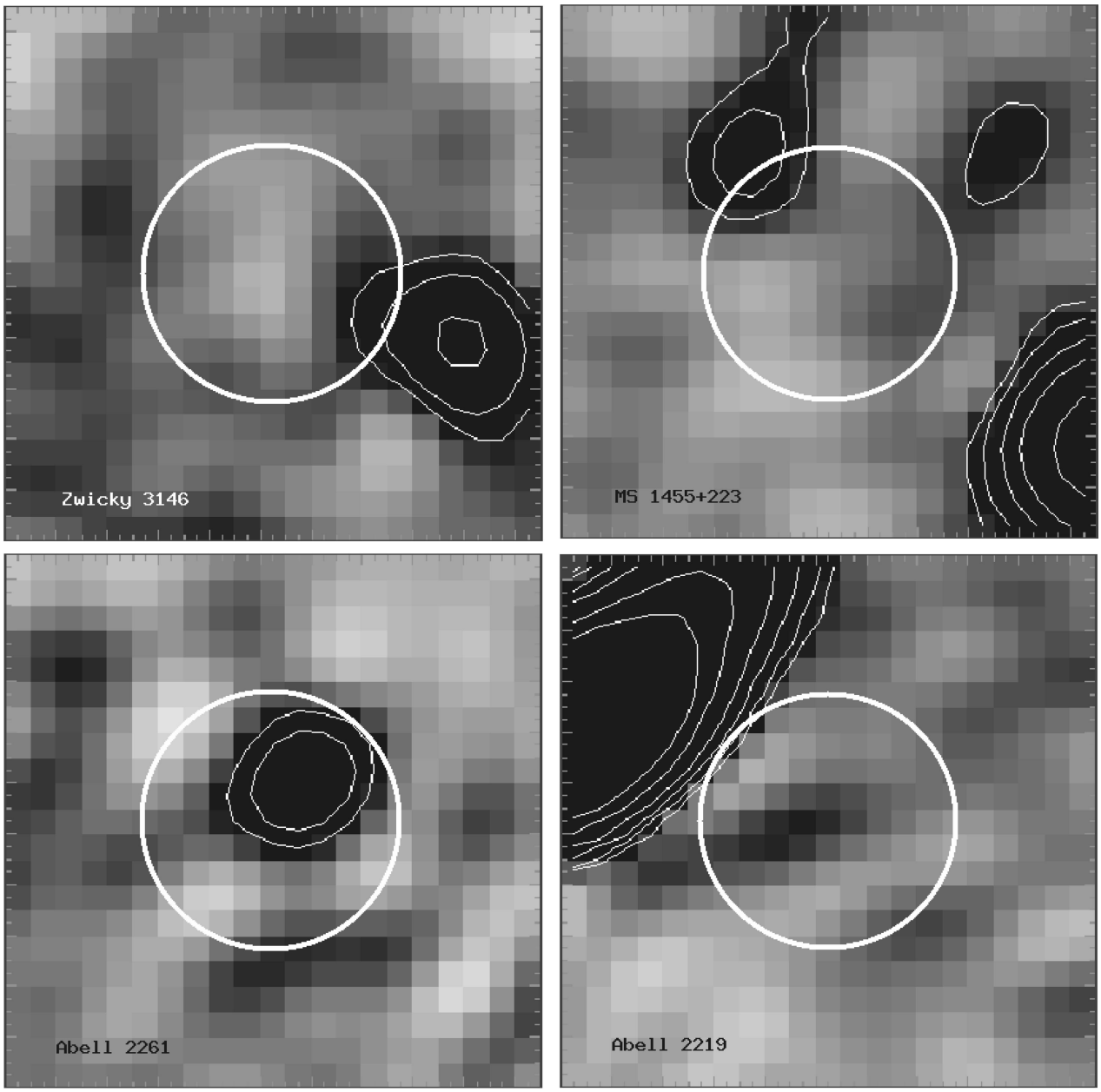

Figure 4. VLA 4.9-GHz maps surrounding the brightest cluster galaxies in Zw 3146, MS 1455, A2261 and A2219. The field size is 21×21 arcsec^2 in all cases. Radio contours are 3, 5, 10, 20, 50 and 100 times the rms of the VLA map region. A 10-arcsec-diameter error circle is overlaid to indicate the SCUBA beam position, for these marginal $2–3\sigma$ 850-μm detections.

are, in addition to the 850-μm detections, two 450-μm detections at the 3σ level. The 1350/850- and 450/850 − μm ratios and lack of a 4.9-GHz detection for source A (SMMJ 16403 + 46440) are consistent with the high redshift predicted from CY. This is the only source in A2219 that does not have at least positive flux density in the VLA archive map. The central source (C: SMMJ 16404 + 4643) is $\simeq 2.2\sigma$ at 850μm but has a fairly clear detection at 450μm. It does not quite align with the central galaxy radio emission (see Fig. 4), but within errors it is possible that the source is a cluster member. Indeed, the large implied 450/850 − μm flux density ratio is indicative of a rather low-redshift source. In the archive 1.4-GHz map, however, there is a 5σ source lying near the SCUBA centroid, offset ∼7 arcsec from the BCG. Source D (SMMJ 16404 + 4644) lies near the edge of the frame (and off the 450-μm frame entirely), and is only 3σ above the local noise level. However, the centroid is within 5 arcsec of an *ISO* 15-μm source (Barvainis, Antonucci & Helou 1999), with which the submillimetre source may be associated.

4.2.9 Abell 2261

Although the bright ($> 4\sigma$) source to the west (A: SMMJ 17223 + 3207) does not correspond with any radio emission, the central 2.5σ peak in the SCUBA map is identified with a radio source coincident with the optical BCG (Fig. 4). An additional 850-μm photometry observation centred on source A reveals a detection of 13.6 ± 2.8 mJy, which is consistent within the relative errors between the mapping and photometry measurements, as well as the extended nature of this source and positional uncertainties.

4.3 Cooling flows and centrally concentrated dust emission

The high central densities of the X-ray gas in many luminous clusters lead to predicted cooling times shorter than the Hubble time (e.g. Fabian 1994). This cooling gas, which cannot support the pressure exerted by the overlying hot gas, is expected to flow into the cluster centre. Supporting evidence for such cooling flows is now available in the form of inverted X-ray temperature profiles (e.g. Buote 1999), and X-ray emission lines show gas that has lost most of its thermal energy. The fate of this cool gas remains controversial (e.g. Braine & Dupraz 1994) as no sink has yet been clearly identified.

Observations of the central cluster galaxies in cooling flow clusters indicate that the cooling flows are not forming large numbers of stars. On the other hand, such stars could be hidden if the initial mass function is biased towards low masses, making the integrated stellar spectrum difficult to detect (e.g. Fabian, Nulsen & Canizares 1982; Mathews & Brighenti 1999). However, the emission-line nebulosity around the central galaxies in many cooling flow clusters, seen on scales of up to 100 kpc, has emission-line ratios suggestive of large amounts of dust in the central regions – this dust could obscure any stars formed there (Hansen, Jörgensen & Nörgaard-Nielsen 1995; Allen et al. 1995). *HST* imaging of central cluster galaxies (e.g. for Abell 1795: McNamara et al. 1996; Pinkney et al. 1996; for Abell 2597: Koekemoer et al. 1999) has also directly detected dust lanes in some cases. At present the total amount or temperature of this dust is difficult to estimate from the scant observational evidence. Whether the observed dust originates from the cooled gas clouds themselves or from the on-going star formation remains unknown.

SCUBA data may help here by probing emission from cool dust in or around the central galaxies in clusters. Both dust and rotational transitions of the CO molecule are tracers of the cool gas (there is approximately one CO molecule for every 10^4 H_2 molecules), and, as such, both must depend on metallicity in some way. The implications of detected cool dust in the BCGs of massive clusters for the interpretation of star formation in cooling flow galaxies has been discussed by Annis & Jewitt (1993) and Edge et al. (1999). Although there are no highly significant detections of the BCGs in our sample, three of the clusters show a marginal positive flux density at 850μm ($\sim 2.5\sigma$) near the BCG. In Abell 2219, a 3.5σ detection at 450μm (2.3σ at 850μm) lies very near a radio-luminous BCG (Fig. 4). In addition, the cluster MS 0451 shows an extended 4σ detection near the X-ray centroid (Donahue 1996), although the BCG is offset from this position by 23 arcsec, and the only radio source in the vicinity is offset to the other side by 20 arcsec. Radio maps of the four cluster centres with possible BCG detection, along with 10-arcsec submillimetre error circles for reference, are shown in Fig. 4.

Molecular gas, traced by CO emission, might also be present in strong cooling flows (Braine et al. 1995). For MS 1455, we also obtained an upper limit on the CO(4–3) emission from the BCG, which suggests a gas-to-dust ratio of $\lesssim 150$ if the SCUBA peak is actually a detection. This would be somewhat unusual for known properties of dusty BCGs (Edge et al. 1999), but a weak CO(1–0) detection for the MS 1455 BCG (A. Edge, private communication) lends support to a possible SCUBA detection.

If the SCUBA detection in MS 0451 is associated with a cooling flow, then it is fairly unusual, and may indicate that a massive but highly obscured optical counterpart is actually being built by cooling flow fallout at the true centre of the cluster potential.

We can place limits on the dust mass for the BCG for all clusters in our sample, by considering the 850-μm flux density limit at the redshift of the BCG (see Edge et al. 1999), and adopting model dust parameters, for example $T_d = 40$ K, with an emissivity index of 1.5. These limits, along with the position of the BCG, are presented in Table 3. CO(1–0) detections for six cooling flow clusters and limits for nine others, as well as broader implications for cooling flows, are presented by Edge et al. (2001). Our limits to the dust mass can be converted to total gas mass by taking a Galactic dust-to-gas ratio (∼ 500) and assuming that the corresponding neutral and molecular gas masses are approximately equal. The limits are generally much less than the total mass deposition implied by the cluster cooling flows. However, our observations are restricted to emission around the BCG, and in any case the limits are model-dependent.

Any conclusions that we draw must necessarily not be very strong. Our non-detections, or relatively weak submillimetre emission, from most BCGs in a sample of nine clusters imply that substantial effort will be required to detect other central cluster galaxies, and that if some of the mass is being deposited as cool dust, this will be hard to detect in typical central cluster galaxies with current instrumentation.

5 SOURCE COUNTS

Source count models for rich cluster fields in the submillimetre have been studied in detail by Blain (1997) and Blain et al. (1999a), with observational constraints presented by Smail et al. (1997) and Ivison et al. (2000). For unmagnified blank fields, the submillimetre galaxy counts can be derived by simply dividing the number of detected sources by the surveyed area, although the effects of clustering may have to be considered in small fields (Scott & White 1999). The situation is more complicated in the case of lensing

caused by a massive cluster, since the source plane is both distorted and magnified at a level dictated by the source redshift and position. Thus in the image plane various regions are observed to different depths. Although our clusters were not chosen to provide the largest lensing amplification, the models of Blain (1997, fig. 4) show that our cluster redshifts are essentially optimal for maximum amplification, with the exception of MS 1054 which has slightly too high a redshift, but still incurs a reasonably large lensing amplification.

We model the amplification for each source and the effective depth of the source plane area observed using an elliptical potential model of each cluster (Korman, Schneider & Bartelmann 1994; Newbury 1997). Parameters for the models are derived both from our own imaging data and from the best current information available in the literature. The lensing inversion is based on the prescription of Korman et al. (1994) and Newbury & Fahlman (1999), allowing a calculation of the lensing amplification and distortion as a function of position in the image plane. Table 4 presents the parameters for each cluster along with an estimate for the lensing amplification at each source position. Columns list the cluster name, redshift, cluster velocity dispersion, angular distance and position angle from north of each source relative to the X-ray centroid, and resulting lens amplification. The final column lists the reference for the cluster parameters. All distances assume a flat Λ-dominated cosmology with $\Omega_{\rm M} = 0.3$.

The essential parameters of the model are the redshift of the cluster and the 1D (line-of-sight) velocity dispersion (σ_V), the latter being essential for setting the mass scale. These two quantities set the length scale in the image plane. Larger cluster redshifts reduce the effective magnification, while larger cluster velocity dispersions (cluster mass) increase the magnification. Although more detailed mass models can in principle be constructed using the radial velocities of the individual cluster members (see Blain et al. 1999a), the errors in the source counts are of the order of 30 per cent, and our results would be very little affected by the use of such cluster mass models.

There is still an ambiguity associated with the unknown background source redshift. However, the models can be used to constrain the range of possible magnifications. For sources at reasonably large redshift ($z > 1$, say), we find that the cumulative source counts depend fairly weakly on the actual source redshift (less than 30 per cent scatter) in agreement with Blain et al. (1999a). If all sources are assumed to lie at $z > 2$, the scatter reduces further. We assume for simplicity that all sources lie at $z = 2$. Based on our CY radio analysis of the source redshifts, this is a reasonable assumption, although some sources may in fact lie at somewhat lower redshifts, especially if their dust temperatures are lower than 50 K.

The cluster ellipticity (E) is chosen based on an outer contour for the central galaxy, if one exists. In the absence of this BCG contour, we assume circular symmetry. The ellipticity is important only in the case of sources near the cluster centre such as in Zw 3146. The core radius ($R_{\rm core}$) of the cluster is a model-dependent parameter – the core radius of the X-ray gas being temperature-dependent. However, for clusters with lensed arcs in their image, it is possible to estimate the core radius directly. Again, the magnification is particularly sensitive to this number only near the cluster centre, as it sets the location of the critical lines with very large magnification. The ellipticity and core radius are quasi-independent parameters of the models. For modest values

Table 3. Limits on dust mass for central cooling flows.

Cluster	RA[a] (J2000)	Dec.[a] (J2000)	S_{850}[b] (mJy)	S_{450}[b] (mJy)	Dust mass[c] $h_{50}^{-2}\,{\rm M}_\odot$
CL 0016 + 16	00 18 33.2	+ 16 26 18	<6.1	<66	$<4.2\times10^8$
MS 0451−03	04 54 13.4	− 03 01 47	19.1 ± 4.2	<354	1.3×10^9
Abell 520	04 54 19.0	+ 02 56 49	<10.0	<116	$<2.5\times10^8$
Zwicky 3146	10 23 39.6	+ 04 11 10	6.6 ± 2.6	<48	2.4×10^8
MS 1054−03	10 56 06.2	− 03 37 27	<8.4	<203	$<8.5\times10^8$
MS 1455 + 22	14 57 15.1	+ 22 20 35	5.3 ± 2.1	<42	1.5×10^8
Abell 2163	16 15 34.1	− 06 07 26	<11.3	<86	$<3.1\times10^8$
Abell 2219	16 40 20.5	+ 46 42 59	3.6 ± 1.7	26 ± 8	9.0×10^7
Abell 2261	17 22 24.1	+ 32 07 45	9.5 ± 3.8	<205	1.8×10^8

[a] BCG position.
[b] Where no positive value $>2.0\sigma$ is detected, we quote Bayesian 95 per cent upper limits.
[c] Assuming $T_{\rm d} = 40$ K and $\beta = 1.5$, with $h_{50}H_0/100\,{\rm km\,s^{-1}\,Mpc^{-1}}$.

Table 4. Lensing parameters for clusters.

Cluster	z	σ_V(km s^{-1})	$\Delta\theta_{\rm source}$ (PA)[a]	Lens amplification	Cluster reference
Cl 0016 + 16	0.541	1243	44(138), 62(171)	3.0, 2.6	Ellingson et al. (1998)
MS 0451 − 03	0.550	1353	65(130), 25(46)	2.6, 4.5	Donahue (1996)
Abell 520	0.203	927	61(104), 74(138)	3.4, 3.1	Gioia & Luppino (1994)
Zwicky 3146	0.291	1310	31(117), 62(179), 69(−33), 78(−136)	6.8, 3.7, 3.5, 3.2	Ebeling et al. (1996)
MS 1054 − 03	0.833	1170	63(70)	2.6	Donahue et al. (1998)
MS 1455+22	0.259	1168	58(162.5)	2.8	Stocke et al. (1991)
Abell 2163	0.201	1231	n/a	n/a	Gioia & Luppino (1994)
Abell 2219	0.228	1000	66(17), 45(157), 15(178), 41(−93)	3.6, 3.2, 7.5, 3.0	Smail et al. (1996)
Abell 2261	0.224	1102	72(−124)	3.3	Ebeling et al. (1996)

[a]Distance and position angle of the sources (listed in Table 2) from the X-ray centre.

of the ellipticity, this parameter plays a very small role, especially in view of all the other uncertainties involved.

Lensing increases the brightness of sources and also magnifies the area – so we reach to fainter effective flux limits, but over a smaller effective solid angle. Fig. 5 shows the resulting magnification versus source plane area for each cluster. Our complete survey area in the source plane is in fact only ~ 19 arcmin^2, from a total surveyed SCUBA field area of ~ 47 arcmin^2. We estimate that the uncertainties in cluster parameters (σ_v, $R_{\rm core}$, E) for the lensing model contribute ~ 25 per cent error, a little larger than the errors in calibrating SCUBA maps, but less than the Poisson error in the source counts themselves.

6 RESULTS

With the lensing factored in, our effective noise level in the central regions of the cluster fields decreases sharply, as displayed in Fig. 6. From these relations of sensitivity as a function of cluster area, we can calculate the effective area surveyed to a given depth. Fig. 7 shows the integral source counts from our survey including all sources detected at $>3\sigma$ (solid circles, binned). We plot the counts from the Smail et al. (1997) lensing survey presented by Blain et al. (1999c, crosses), as well as a fit to the combined blank field submillimetre counts (Hughes et al. 1998; Barger et al. 1999b; Eales et al. 1999) constrained at faint fluxes not to overproduce the far-infrared background (dotted line). When we restrict ourselves to the $>4\sigma$ subset which contains no obvious cluster members, there is no dramatic change in the counts (open circles in Fig. 7). We fit these 4σ counts with a simple power law $N(>S) = N_0(SS_0)^{-\gamma}$, with $S_0 = 1$ mJy, and find $\gamma \simeq 1.73$ and $N_0 \simeq 11200$. These are close to the blank field values of $\gamma = 2.2$ and $N_0 = 13600$. A direct comparison with other published submillimetre source counts thus reveals a good agreement between results, consistent within 1σ error bars, including gravitationally lensed and blank field counts. SCUBA preferentially selects galaxies with $z \gtrsim 1$, owing to the spectral shape at these wavelengths. Therefore we expect few detections in the clusters themselves; however, this may be the source of some of the small discrepancy between the various surveys.

A positive magnification from the cluster lensing means that we are seeing fainter galaxies, and hence an increase in the surface density of galaxies. However, this is offset by the loss in area

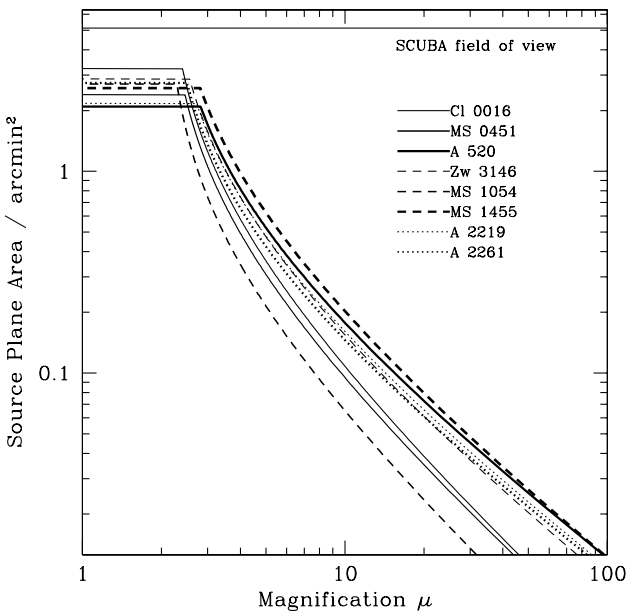

Figure 5. Area versus amplification in the source plane for the eight clusters in our sample with detected sources.

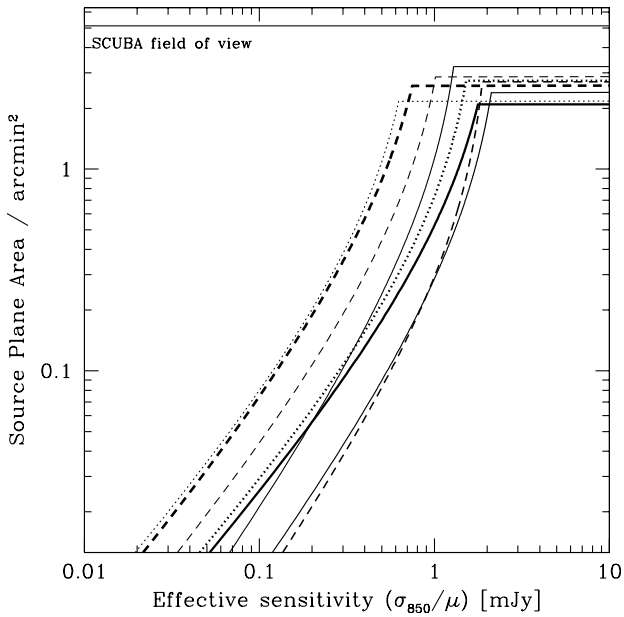

Figure 6. Area versus sensitivity for the eight clusters in our sample with detected sources. Line types are the same as in Fig. 5.

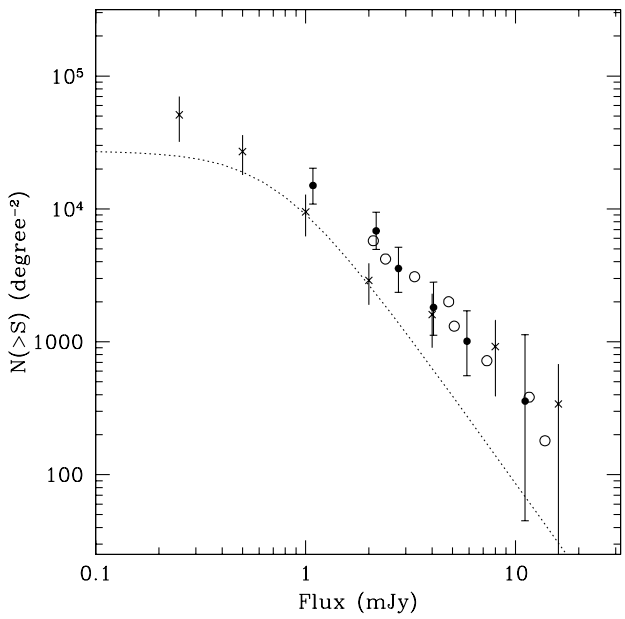

Figure 7. The integral source counts (number of objects brighter than flux density S) as a function of S. We plot our total counts of $>3\sigma$ detections (solid circles, binned), and our subsample excluding possible cluster members and detections of less than 4σ significance (open circles, individual sources). The corrected counts from Blain et al. (1999c) are plotted with crosses. The dotted line depicts a fit to the combined blank field submillimetre counts (Hughes et al. 1998; Barger et al. 1999b; Eales et al. 1999) constrained at faint fluxes not to overproduce the far-infrared background. The error bars shown for our complete sample points are $\pm 1\sigma$ (68 per cent Bayesian confidence region) errors based on Poisson statistics.

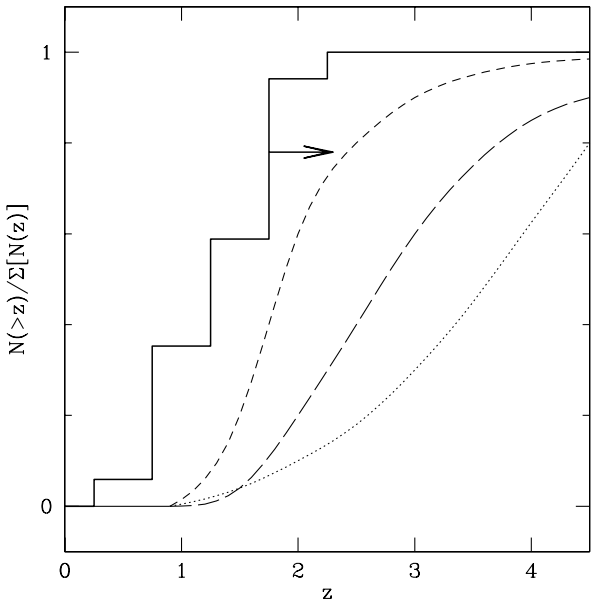

Figure 8. Cumulative redshift distribution estimated for our entire sample, derived from the CY relation using VLA data (solid line). Also shown are the cumulative redshift distributions for models formulated to fit the far-infrared background, and various infrared counts: Guiderdoni et al. (1998) (dotted line), the Blain et al. (1999b) Gaussian model of luminosity evolution (long-dashed line); and the Blain et al. (1999b) modified Gaussian model fit to the Barger et al. (1999a) redshift distribution (short-dashed line).

arising from field distortion. If the source count power-law index were too shallow, this would result in a less efficient survey compared with a blank field survey with equivalent integration time. However, our results show a net positive bias, so that we are detecting more sources per unit time and at unlensed flux densities below what would be possible in blank field searches, in line with what was found earlier by Smail et al. (1997).

Using the amplification arising from the foreground cluster, lensed surveys also suffer less from confusion noise (e.g. Blain et al. 1998). The large beamsize of SCUBA implies a confusion limit at ~ 1.5 mJy, while we have detected four possible sources fainter than 2 mJy.

7 DISCUSSION

Estimates of the redshift distribution for the SCUBA-selected sources remain in dispute (Hughes et al. 1998; Barger et al. 1999a; Lilly et al. 1999a). Hughes et al. (1998) concluded that the bulk of the population is at $z \sim 2$–4, based on photometric redshift limits for the probable counterparts of five submillimetre sources in the *Hubble Deep Field* (cf. Richards 1999; Downes et al. 1999). Barger et al. (1999a) undertook a spectroscopic survey of the Smail et al. (1999) submillimetre sample and concluded that the median redshift was ~ 1.5–2, with the bulk of the population having $z \sim 1$–3. Lilly et al. (1999a) used archival spectroscopy and broad-band photometry of submillimetre sources from the Eales et al. (1999) survey to conclude that the population spans $z = 0.1$–3, with a third at $z < 1$. Given the relatively small number statistics and the very real possibility of some misidentifications, it is unclear whether there is any genuine disagreement.

However, use of the Carilli & Yun (2000, CY) relation of radio/far-infrared flux to predict the redshifts for a large sample of SCUBA sources (Smail et al. 2000) has suggested that the population may have a median value lying between $z = 2.5$ and 3. This is consistent with our CY analysis using VLA maps, which result in a median value lying at $z \gtrsim 2.0$, although dependent on the dust temperature and emissivity adopted. Fig. 8 shows an estimate of the cumulative redshift distribution for our entire sample, derived from the CY relation using radio detections and lower limits. Also depicted are the cumulative redshift distributions for models formulated to fit the far-infrared background, and various infrared counts, by Guiderdoni et al. (1998) and Blain et al. (1999b).

The archival radio maps for many of our cluster fields are not deep enough to put strong constraints on the redshift distribution of submillimetre sources, with few actual radio detections. Given that the derived redshifts are generally lower limits, it is difficult presently to discriminate between predictions for the redshift distribution from various models [e.g. the Blain et al. (1999b) model Gaussian and modified Gaussian models (long and short dashes) or the Guiderdoni et al. (1998) model (dotted line)]. However, the radio/far-infrared correlation indicates that the bulk of the dust emission in the Universe did not occur at redshifts much below $z = 2$. The true redshift distribution remains to be determined. Deep optical and near-IR imaging should also uncover the optical properties of these objects, and resolve currently unanswered questions such as whether the galaxies would be detectable through their Lyman break (Chapman et al. 2000), or whether they have extremely red colours (Smail et al. 1999).

We can calculate lower limits to the far-infrared background radiation intensities from measured flux densities of resolved 4σ sources in our cluster fields. The contribution is the sum $\Sigma(SA)$, where A is the area that has a sensitivity necessary to see a source of flux S, where lensing has been factored into the sum. We find 9.1 Jy deg^{-2} averaged over all 9 fields. This corresponds to 20 per cent of the total FIRB at 850μm as measured by Fixsen et al. (1998): 44 Jy deg^{-2}. The accuracy of these estimates, however, depends on the lensing models and other details of the counts, together with the remaining uncertainty in the FIRB measurement at these wavelengths. If we take the simple power-law model integrated up from 1 mJy, then the background is $N_0\gamma/(\gamma - 1)$. Using our slope from Fig. 7 accounts for more than half of the background down to 1 mJy.

8 CONCLUSIONS

Our conclusions are as follows.

(i) We have detected 17 new submillimetre sources in the fields of nine rich galaxy clusters. Comparison with VLA radio images suggests that most of these are being lensed by the cluster mass, rather than being in the clusters themselves.

(ii) We see no strong evidence for cool dust emission around BCGs, which might be related to cooling flows.

(iii) Our submillimetre source counts are in reasonable agreement with existing submillimetre surveys, and extend the list of such sources available for follow-up at other wavelengths.

(iii) The redshift distribution has been loosely constrained using the radio–far-infrared correlation, and favours a relatively high redshift ($z > 2$) for the bulk of dust emission in the Universe.

ACKNOWLEDGMENTS

This work was supported by the Natural Sciences and Engineering Research Council of Canada. The James Clerk Maxwell Telescope is operated by The Joint Astronomy Centre on behalf of the Particle Physics and Astronomy Research Council of the United Kingdom, the Netherlands Organization for Scientific Research, and the National Research Council of Canada. We acknowledge the staff at the JCMT for facilitating these observations. The VLA is run by NRAO and is operated by Associated Universities Inc., under a cooperative agreement with the National Science Foundation.

REFERENCES

Allen S. W., Fabian A. C., Edge A. C., Böhringer H., White D. A., 1995, MNRAS, 275, 741
Andreani P. et al., 1999, ApJ, 513, 23
Annis J., Jewitt D., 1993, MNRAS, 264, 593
Barger A. J., Cowie L., Sanders D., Fulton E., Taniguchi Y., Sato Y., Kawara K., Okuda H., 1998, Nat, 394, 248
Barger A. J., Cowie L., Smail I., Ivison R., Blain A., Kneib J.-P., 1999a, AJ, 117, 2656
Barger A. J., Cowie L. L., Sanders D. B., 1999b, ApJ, 518, L5
Barvainis R., Antonucci R., Helou G., 1999, AJ, 118, 645
Bertoldi F. et al., 2000, A&A, submitted (astro-ph/0006094)
Birkinshaw M., 1999, Phys. Rep., 310, 97
Blain A. W., 1997, MNRAS, 290, 553
Blain A. W., 1999, MNRAS, 309, 955
Blain A., Longair M., 1993, MNRAS, 264, 509
Blain A. W., Ivison R. J., Smail I., 1998, MNRAS, 296, L29
Blain A. W., Smail I., Ivison R. J., Kneib J.-P., 1999a, ApJ, 512, L87
Blain A. W., Smail I., Ivison R. J., Kneib J.-P., 1999b, MNRAS, 302, 632
Blain A. W., Ivison R. J., Kneib J.-P., Smail I., 1999c, in Bunker A. J., van Breugel W. J. M., eds, ASP Conf. Ser. Vol. 193, The Hy-Redshift Universe: galaxy formation and evolution at high redshift. Astron. Soc. Pac., San Francisco, p. 246
Borys C., Chapman S. C., Scott D., 1999, MNRAS, 308, 527
Braine J., Dupraz C., 1994, A&A, 283, 407
Braine J., Wyrowski F., Radford S. J. E., Henkel C., Lesch H., 1995, A&A, 293, 315
Buote D. A., 1999, MNRAS, 309, 685
Carilli C. L., Yun M. S., 1999, ApJ, 513, L13, (CY)
Carilli C. L., Yun M. S., 2000, ApJ, 530, 618, (CY)
Carlstrom J. et al., 1999, in Bergstrom L., Carlson P., Fransson C., eds, Particle Physics and the Universe. World Scientific, Singapore, (astro-ph/9905255)
Chapman S. C., Scott D., Lewis G., Borys C., Fahlman G. G., 1999, A&A, 352, 406
Chapman S. C. et al., 2000, MNRAS, 319, 318
Condon J. J., Yin Q. F., Thuan T. X., Boller T., 1998, AJ, 116, 2682
Crawford C., Allen S., Ebeling H., Edge A., Fabian A., 1999, MNRAS, 307, 91
Donahue M., 1996, ApJ, 468, 79
Donahue M., Voit M., Gioia I., Luppino G., Hughes J., Stocke J., 1998, ApJ, 502, 550
Downes D. et al., 1999, A&A, 347, 809
Dunne L., Clements D., Eales S., 2000, MNRAS, 319, 243
Eales S. A., Lilly S., Gear W., Dunne L., Bond R., Hammer F., Le Fevre O., Crampton D., 1999, ApJ, 518, L641
Eales S., Lilly S., Webb T., Dunne L., Gear W., Clements D., Yun M., 2000, AJ, 120, 2244
Ebeling H., Voges W., Bohringer H., Edge A. C., Huchra J. P., Briel U. G., 1996, MNRAS, 281, 799
Edge A., 2001, MNRAS, 328, 762
Edge A. C., Ivison R. J., Smail I., Blain A. W., Kneib J.-P., 1999, MNRAS, 306, 599
Ellingson E., Yee H. K., Abraham R. G., Morris S. L., Carlberg R., 1998, ApJS, 116, 247
Fabian A. C., 1994, ARA&A, 32, 277
Fabian A. C., Nulsen P. E. J., Canizares C. R., 1982, MNRAS, 201, 933
Fixsen D. J., Dwek E., Mather J. C., Bennett C. L., Shafer R. A., 1998, ApJ, 508, 123
Frayer D., Ivison R. J., Scoville N., Yun M., Evans A., Smail I., Blain A., Kneib J.-P., 1998, ApJ, 506, L7
Frayer D. et al., 1999, ApJ, 514, L13
Frayer D., Smail I., Ivison R. J., Scoville N. Z., 2000, AJ, 120, 1668
Gear W. K., Lilly S. J., Stevens J. A., Clements D. L., Webb T. M., Eales S. A., Dunne L., 2000, MNRAS, 316, L51
Gioia I. M., Luppino G. A., 1994, ApJS, 94, 583
Guiderdoni B., Bouchet F. R., Puget J.-L., Lagache G., Hivon E., 1997, Nat, 390, 257
Guiderdoni B., Hivon E., Bouchet F. R., Maffei B., 1998, MNRAS, 295, 877
Hansen L., Jörgensen H. E., Nörgaard-Nielsen H. U., 1995, A&A, 297, 13
Hauser M. G. et al., 1998, ApJ, 508, 25
Holland W. S. et al., 1999, MNRAS, 303, 659
Hughes D. H. et al., 1998, Nat, 394, 241
Ivison R. J. et al., 1998a, ApJ, 494, 211
Ivison R. J., Smail I., Le Borgne J.-F., Blain A. W., Kneib J.-P., Bezecourt J., Kerr T. H., Davies J. K., 1998b, MNRAS, 298, 583
Ivison R. J. et al., 2000, MNRAS, 315, 209
Jenness T., Lightfoot J. F., Holland W. S., 1998, Proc. SPIE 3357, 548
Koekemoer A. M., O'Dea C. P., Sarazin C. L., McNamara B. R., Donahue M., Voit G. M., Baum S. A., Gallimore J. F., 1999, ApJ, 525, 621
Korman P., Schneider P., Bartelmann M., 1994, A&A, 284, 285
Lagache G., Abergal A., Boulanger F., Desert F. X., Puget J.-L., 1999, A&A, 344, 322
Lilly S. J., Eales S. A., Gear W. K. P., Hammer F., Le Fevre O., Crampton D., Bond J. R., Dunne L., 1999a, ApJ, 343, 123
Lilly S. J., Eales S. A., Gear W. K., Webb T. M., Bond J. R., Dunne L., 1999b, in Carollo C. M., Ferguson H. C., Wyse R. F. G., eds, Formation of Galactic Bulges. Cambridge Univ. Press, Cambridge, p. 119
McNamara B. R., Wise M., Sarazin C. L., Jannuzi B. T., Elston R., 1996, ApJ, 466, L9
Mathews W. G., Brighenti F., 1999, ApJ, 526, 114
Newbury P., 1997, PhD thesis, University of British Columbia
Newbury P., Fahlman G. G., 2001, in Brainerd T. G., Kochanek C. S., eds, ASP Conf. Ser. Vol. 237, Gravitational Lensing: Recent Progress and Future Go. Astron. Soc. Pac., San Francisco, p. 331
Pinkney J. et al., 1996, ApJ, 468, L13
Puget J.-L., Abergel A., Bernard J.-P., Boulanger F., Burton W. B., Desert F.-X., Hartmann D., 1996, A&A, 308, L5
Richards E. A., 1999, ApJ, 513, L9
Richards E., Kellermann K. I., Fomalont E. B., Windhorst R. A., Partridge R. B., 1998, AJ, 116, 1039
Richards E. A., Fomalont E. B., Kellermann K., 1999, ApJ, 526, L71
Sanders D. B., 1999, in Matsumoto T., de Graauw T., eds, Space Infrared Telescopes and Related Science, 32nd COSPAR workshop, Vol. 194, p. 25
Sanders D. B., Mirabel I. F., 1996, ARA&A, 34, 749
Scott D., White M., 1999, A&A, 346, 1
Smail I., Dressler A., Kneib J-P., Ellis R. S., Couch W., 1996, ApJ, 469, 508
Smail I., Ivison R. J., Blain A. W., 1997, ApJ, 490, L5
Smail I., Ivison R. J., Blain A. W., Kneib J.-P., 1998, ApJ, 507, L21
Smail I., Ivison R. J., Kneib J.-P., Cowie L. L., Blain A. W., Barger A. J., Owen F. N., Morrison G., 1999, MNRAS, 308, 1061
Smail I., Ivison R. J., Owen F. N., Blain A. W., Kneib J.-P., 2000, ApJ, 528, 612
Stocke J. T. et al., 1991, ApJS, 76, 813
Stocke J. T., Perlman E. S., Gioia I. M., Harvanek M., 1999, AJ, 117, 1967

This paper has been typeset from a TEX/LATEX file prepared by the author.